# Supplementary Information

# Rapid, artifact-reduced, image reconstruction for super-resolution structured illumination microscopy

Zhaojun Wang[1], Tianyu Zhao[1], Yanan Cai[2], Jingxiang Zhang[1], Huiwen Hao[3], Yansheng Liang[1], Shaowei Wang[1], Yujie Sun[3], Tongsheng Chen[4], Piero R. Bianco[5], Kwangsung Oh[6], Ming Lei[1,*]

[1] MOE Key Laboratory for Nonequilibrium Synthesis and Modulation of Condensed Matter, School of Physics, Xi'an Jiaotong University, Xi'an 710049, China

[2] College of Science, Northwest A&F University, Yangling 712100, China

[3] State Key Laboratory of Membrane Biology & Biomedical Pioneer Innovation Center (BIOPIC) & School of Life Sciences, Peking University, Beijing 100871, China

[4] MOE Key Laboratory of Laser Life Science & Guangdong Provincial Key Laboratory of Laser Life Science, College of Biophotonics, South China Normal University, Guangzhou 510631, China

[5] Department of Pharmaceutical Sciences, College of Pharmacy, University of Nebraska Medical Center, Omaha, NE 68198-6025, USA

[6] Department of Computer Science, College of Information Science & Technology, University of Nebraska Omaha, Omaha, NE 68182, USA

*Correspondence: ming.lei@mail.xjtu.edu.cn

# Supplementary Note 1. Principle of JSFR-AR-SIM

In this note, we first make a brief review on the principle of the widely-used Wiener-SIM algorithm. Afterward, the motivation and principle of HiFi-SIM and JSFR-SIM are respectively discussed in detail, based on which we will further clarify the principle of the new JSFR-AR-SIM.

### 1.1 Basic principle of the conventional Wiener-SIM algorithm

For conventional SR-SIM, the raw images acquired with three equally spaced phase shifts in three orientations can be modeled as

$$\begin{aligned} D_{d,i}(\mathbf{r}) &= \left[O(\mathbf{r})\bullet I_{d,i}(\mathbf{r})\right]\otimes H(\mathbf{r}) \\ &= \left\{O(\mathbf{r})\bullet[1+m_d\cos(\mathbf{k}_d\bullet\mathbf{r}+\varphi_{d,i})]\right\}\otimes H(\mathbf{r}) \end{aligned} \tag{1}$$

where **r** indicates the spatial coordinates in three dimensions, $O(\mathbf{r})$ denotes the distribution of the specimen, $I(\mathbf{r})$ represents the intensity distribution of the sinusoidal excitation patterns, $m_d$ is modulation depth of the illumination pattern, $H(\mathbf{r})$ indicates the point spread function of the optical microscopy, $\mathbf{k}_d$ and $\varphi_{d,i}$ are respectively the wavenumber and the phase of the excitation pattern, and the subscripts $d$ (=1,2,3) and $i$ (=1,2,3) respectively denote the index of the pattern orientation and the phase shifts.

In the workflow of conventional Wiener-SIM, these raw images are first transformed to the frequency domain as follows

$$\begin{aligned} \tilde{D}_{d,i}(\mathbf{k}) &= \left\{\tilde{O}(\mathbf{k})+m_d\tilde{O}(\mathbf{k})\otimes\mathscr{F}[\cos(\mathbf{k}_d\bullet\mathbf{r}+\varphi_{d,i})]\right\}\bullet\tilde{H}(\mathbf{k}) \\ &= \tilde{O}(\mathbf{k})\tilde{H}(\mathbf{k})+\frac{m_d e^{i\varphi_{d,1}}}{2}\tilde{O}(\mathbf{k}-\mathbf{k}_d)\tilde{H}(\mathbf{k})+\frac{m_d e^{-i\varphi_{d,1}}}{2}\tilde{O}(\mathbf{k}+\mathbf{k}_d)\tilde{H}(\mathbf{k}) \end{aligned} \tag{2}$$

where **k** denotes the frequency coordinates, $\tilde{D}_{d,i}(\mathbf{k})$ represents the raw images in the Fourier domain, and $\tilde{B}_{d,i}(\mathbf{k})$ is the spectrum of the background fluorescence in the raw images. To solve the three spectrum components of the specimen, the illumination patterns are laterally shifted, with which an equation set can be easily constructed

$$\begin{bmatrix} 1 & m_d e^{i\varphi_{d,1}}/2 & m_d e^{-i\varphi_{d,1}}/2 \\ 1 & m_d e^{i\varphi_{d,2}}/2 & m_d e^{-i\varphi_{d,2}}/2 \\ 1 & m_d e^{i\varphi_{d,3}}/2 & m_d e^{-i\varphi_{d,3}}/2 \end{bmatrix} \begin{bmatrix} \tilde{O}(\mathbf{k})\tilde{H}(\mathbf{k}) \\ \tilde{O}(\mathbf{k}-\mathbf{k}_d)\tilde{H}(\mathbf{k}) \\ \tilde{O}(\mathbf{k}+\mathbf{k}_d)\tilde{H}(\mathbf{k}) \end{bmatrix} = \begin{bmatrix} \tilde{D}_{d,1}(\mathbf{k}) \\ \tilde{D}_{d,2}(\mathbf{k}) \\ \tilde{D}_{d,3}(\mathbf{k}) \end{bmatrix} \tag{3}$$

By carefully choosing the phase shifts (to guarantee the 3×3 matrix in Eq. (3) to be full-rank), the spectrum components can be solved with above the equation set, after the illumination pattern parameters $\mathbf{k}_d$, $\varphi_{d,i}$, $m_d$ are determined.

Denoting the 0-order and ±1$^{st}$-order components of the specimen as $\tilde{S}_{d,0}(\mathbf{k})$, and $\tilde{S}_{d,\pm1}(\mathbf{k})$

$$
\begin{aligned}
&\tilde{S}_{d,0}(\mathbf{k}) = \tilde{O}(\mathbf{k})\tilde{H}(\mathbf{k}) \\
&\tilde{S}_{d,+1}(\mathbf{k}) = \tilde{O}(\mathbf{k})\tilde{H}(\mathbf{k}+\mathbf{k}_d) \\
&\tilde{S}_{d,-1}(\mathbf{k}) = \tilde{O}(\mathbf{k})\tilde{H}(\mathbf{k}-\mathbf{k}_d)
\end{aligned}
\tag{4}
$$

We have

$$
\begin{bmatrix} \tilde{S}_{d,0}(\mathbf{k}) \\ \tilde{S}_{d,+1}(\mathbf{k}-\mathbf{k}_d) \\ \tilde{S}_{d,-1}(\mathbf{k}+\mathbf{k}_d) \end{bmatrix} = \begin{bmatrix} 1 & m_d e^{i\varphi_{d,1}}/2 & m_d e^{-i\varphi_{d,1}}/2 \\ 1 & m_d e^{i\varphi_{d,2}}/2 & m_d e^{-i\varphi_{d,2}}/2 \\ 1 & m_d e^{i\varphi_{d,3}}/2 & m_d e^{-i\varphi_{d,3}}/2 \end{bmatrix}^{-1} \begin{bmatrix} \tilde{D}_{d,1}(\mathbf{k}) \\ \tilde{D}_{d,2}(\mathbf{k}) \\ \tilde{D}_{d,3}(\mathbf{k}) \end{bmatrix}
\tag{5}
$$

Afterward, an expanded spectrum of the sample can be recovered by shifting higher frequencies to the correct position in frequency space and combining the results

$$
\tilde{S}_{directly-conbined}(\mathbf{k}) = \sum_{d=1}^{3} \left[ \tilde{S}_{d,0}(\mathbf{k})\tilde{H}^*(\mathbf{k}) + \tilde{S}_{d,+1}(\mathbf{k})\tilde{H}^*(\mathbf{k}+\mathbf{k}_d) + \tilde{S}_{d,-1}(\mathbf{k})\tilde{H}^*(\mathbf{k}-\mathbf{k}_d) \right]
\tag{6}
$$

Consequently, deconvolution and apodization are applied to increase the spatial resolution and suppress high-frequency related artifacts

$$
I_{\text{Wiener-SIM}}(\mathbf{k}) = \tilde{S}_{directly-conbined}(\mathbf{k}) * \tilde{W}_0(\mathbf{k})
\tag{7}
$$

$$
\tilde{W}_0(\mathbf{k}) = \frac{\tilde{A}(\mathbf{k})}{\left\{ \sum_{d=1}^{3} \left[ \left|\tilde{H}(\mathbf{k})\right|^2 + \left|\tilde{H}(\mathbf{k}+\mathbf{k}_d)\right|^2 + \left|\tilde{H}(\mathbf{k}-\mathbf{k}_d)\right|^2 \right] \right\} + w^2}
\tag{8}
$$

where $w$ is an empirical parameter of the Wiener filter, and $\tilde{A}(\mathbf{k})$ is the apodization function, which shares a similar shape with the OTF but the cutoff frequency is extended to $|\boldsymbol{k}_c|+|\boldsymbol{k}_d|$. The final SR image can be obtained by transforming the spectrum back into real space.

The above reconstruction workflow works fine in situations where the background fluorescence is subtle. However, for the majority of eukaryotic cells, the organelles often spread over several microns thickness, which imposes intense background information on the raw images. Consequently, each separated component in Eq. (5) should be revised by appending an additional term

$$
\begin{aligned}
&\tilde{S}_{d,0}(\mathbf{k}) = \tilde{O}(\mathbf{k})\tilde{H}(\mathbf{k}) + \tilde{b}_{d,0}(\mathbf{k}) \\
&\tilde{S}_{d,+1}(\mathbf{k}) = \tilde{O}(\mathbf{k})\tilde{H}(\mathbf{k}+\mathbf{k}_d) + \tilde{b}_{d,+1}(\mathbf{k}+\mathbf{k}_d) \\
&\tilde{S}_{d,-1}(\mathbf{k}) = \tilde{O}(\mathbf{k})\tilde{H}(\mathbf{k}-\mathbf{k}_d) + \tilde{b}_{d,-1}(\mathbf{k}-\mathbf{k}_d)
\end{aligned}
\tag{9}
$$

in which the additional terms $\tilde{b}_{d,i}(\mathbf{k})$ can be expressed as follows

$$\begin{bmatrix} \tilde{b}_{d,0}(\mathbf{k}) \\ \tilde{b}_{d,+1}(\mathbf{k}) \\ \tilde{b}_{d,-1}(\mathbf{k}) \end{bmatrix} = \begin{bmatrix} 1 & m_d e^{i\varphi_{d,1}}/2 & m_d e^{-i\varphi_{d,1}}/2 \\ 1 & m_d e^{i\varphi_{d,2}}/2 & m_d e^{-i\varphi_{d,2}}/2 \\ 1 & m_d e^{i\varphi_{d,3}}/2 & m_d e^{-i\varphi_{d,3}}/2 \end{bmatrix}^{-1} \begin{bmatrix} \tilde{B}_{d,1}(\mathbf{k}) \\ \tilde{B}_{d,2}(\mathbf{k}) \\ \tilde{B}_{d,3}(\mathbf{k}) \end{bmatrix} \tag{10}$$

where $\tilde{B}_{d,i}(\mathbf{k})$ is the spectrum of the background fluorescence in each raw image.

Considering the background mostly contributes to the low-frequency components, these additional terms will present a spectrum spike at the zero-position in frequency coordinates. After moving these components to their proper position, the spectrum spike located at zero-position will also be moved to $\pm\mathbf{k}_d$, which results in six spectrum spikes (3×2) in the final spectrum[1]. These spikes are the source of the honeycomb artifacts induced by thick specimens.

To restrain the out-of-focus background and the honeycomb artifacts, the OTF attenuation method proposed by O'Holleran et al. is widely used in SIM communities[1], which maximizes the axial frequency extent of the combined 2D structured illumination passband by attenuating the shifted spectrum components with the following equation

$$\begin{aligned} \tilde{S}_{directly-conbined}(\mathbf{k}) = \sum_{d=1}^{3} [ & a(\mathbf{k})\tilde{H}^*(\mathbf{k})\tilde{S}_{d,0}(\mathbf{k}) + a(\mathbf{k}+\mathbf{k}_d)\tilde{H}^*(\mathbf{k}+\mathbf{k}_d)\tilde{S}_{d,+1}(\mathbf{k}) \\ & + a(\mathbf{k}-\mathbf{k}_d)\tilde{H}^*(\mathbf{k}-\mathbf{k}_d)\tilde{S}_{d,-1}(\mathbf{k})] \end{aligned} \tag{11}$$

where $\mathbf{k}$ denotes the 2-dimensional wave vector in the frequency domain, $\mathbf{k}_d$ represents the wave vector of the structured illumination in $n$th orientation. $a(\mathbf{k})$ is an inversed Gaussian function defined by

$$a(\mathbf{k}) = 1 - A_{\text{att}} e^{-\frac{\mathbf{k}^2}{(0.5\bullet\sigma_{att})^2}} \tag{12}$$

in which the amplitude of the attenuation $A_{\text{att}}$ and the standard deviation of the Gaussian $\sigma_{\text{att}}$ are empirically adjusted parameters.

At the same time, the deconvolution procedure is revised as

$$I_{\text{Wiener-SIM}}(\mathbf{k}) = \tilde{S}_{directly-conbined}(\mathbf{k}) * \tilde{W}_0(\mathbf{k}) \tag{13}$$

$$\tilde{W}_0(\mathbf{k}) = \frac{\tilde{A}(\mathbf{k})}{\left\{ \sum_{d=1}^{3} a(\mathbf{k})\left|\tilde{H}(\mathbf{k})\right|^2 + a(\mathbf{k}+\mathbf{k}_d)\left|\tilde{H}(\mathbf{k}+\mathbf{k}_d)\right|^2 + a(\mathbf{k}-\mathbf{k}_d)\left|\tilde{H}(\mathbf{k}-\mathbf{k}_d)\right|^2 \right\} + w^2} \tag{14}$$

where $w$ denotes the empirical Wiener parameter.

### 1.2 A brief introduction to HiFi-SIM

As is well known, the traditional Wiener-SIM algorithm is prone to reconstruction artifacts because of various reasons[2-4], including improper system configuration, inaccurate parameter estimation, high-frequency noises, and abnormal spectrums. Fortunately, most of these artifacts can be restrained or even eliminated by employing elaborately-calibrated systems and carefully-designed reconstruction algorithms[2,3]. However, the sidelobe artifacts caused by the downward kinks in the OTF were not properly handled for a long time, because it induces an irreconcilable tradeoff between spatial resolution and image fidelity. To address this issue, HiFi-SIM[4] used a two-step spectrum optimization protocol at the final step of the reconstruction, which effectively suppressed common artifacts, without losing fine and weak structures of the specimen.

The reconstruction process of HiFi-SIM mainly differs from the traditional Wiener-SIM in these three aspects. Firstly, as a preprocessing procedure, all the raw images were deconvoluted using the RL deconvolution algorithm with the theoretical OTF. Secondly, an improved normalized cross-correlation method was used to estimate the pattern wave vectors, which can effectively suppress contributions from low-frequency signal and local periodic structures to the cross-correlation map. As the most critical modification, a two-step spectrum optimization was designed for the final deconvolution procedure to suppress the sidelobe artifacts. Thereinto, the first optimization step was designed to suppress the abnormal features and the residual background in the combined spectra, and the subsequent step was aimed at recovering the high-frequency signals suppressed by the optimized OTF.

Among these modifications, the improvement of parameter estimation is an individual portion of the entire reconstruction. The improved estimation method in HiFi-SIM was proven to be more robust in some extreme cases but made little difference in ordinary scenarios where the parameters can be correctly estimated. Therefore, for general applications, we can choose the estimation methods[4-9] according to our preferences, as long as the parameter can be correctly estimated. Considering the performance benchmark of these estimation methods is irrelevant to our major contribution, the detail of parameter estimation will not be further discussed in the following sections for the sake of brevity.

Except for the parameter estimation, the main workflow of HiFi-SIM contains four procedures. Firstly, the raw images were preprocessed with Richardson-Lucy (RL) deconvolution algorithm by employing a theoretical OTF

$$D'_{d,i}(\mathbf{r}) = RL\left[D_{d,i}(\mathbf{r}), H(\mathbf{k}), n\right] \tag{15}$$

where $D_{d,i}(\mathbf{r})$ denotes the raw images, $RL(*)$ represents the RL deconvolution, $H(\mathbf{k})$ is the theoretical OTF of the system, $n$ indicates the number of iterations.

By substituting the spectra of the preprocessed raw images $D'_{d,i}(\mathbf{r})$ into Eq. (5), the 0- and ±1-order spectrum components $\tilde{S}'_{d,0}(\mathbf{k})$, $\tilde{S}'_{d,\pm1}(\mathbf{k})$ could be easily solved. Similar to the conventional Wiener-SIM, a new directly combined spectrum can be obtained by employing OTF attenuation, OTF compensation, band shift, and band superposition

$$\begin{aligned}\tilde{S}'_{directly-conbined}(\mathbf{k}) = \sum_{d=1}^{3}[&a(\mathbf{k})\tilde{H}^*(\mathbf{k})\tilde{S}'_{d,0}(\mathbf{k}) + a(\mathbf{k}+\mathbf{k}_d)\tilde{H}^*(\mathbf{k}+\mathbf{k}_d)\tilde{S}'_{d,+1}(\mathbf{k}) \\ &+a(\mathbf{k}-\mathbf{k}_d)\tilde{H}^*(\mathbf{k}-\mathbf{k}_d)\tilde{S}'_{d,-1}(\mathbf{k})]\end{aligned} \tag{16}$$

Further, the directly-combined spectrum can be optimized by performing a two-step spectrum optimization, which was implemented by replacing the $\tilde{W}_0(k)$ in conventional Wiener-SIM with two specially-designed individual optimization functions $\tilde{W}_1(k)$ and $\tilde{W}_2(k)$. Thereinto,

$\tilde{W}_1(k)$ is designed to construct an initial optimization function to correct the abnormalities of $\tilde{S}'_{directly-conbined}(\mathbf{k})$, where a optimization function is used to modulate all the raised peaks into inverted peaks to remove the residual background signals

$$\tilde{W}_1(\mathbf{k}) = \frac{\tilde{H}_{ideal}(\mathbf{k})}{\sum_m a_1(\mathbf{k}+m\mathbf{k}_d)\bullet\left|\tilde{H}(\mathbf{k}+m\mathbf{k}_d)\right|^2 + w_1^2} \tag{17}$$

where $\tilde{H}_{ideal}(\mathbf{k})$ denotes the ideal OTF of with doubled resolution, $w_1$ represents an empirical parameter for the initial Wiener deconvolution, and $a_1(\mathbf{k})$ is the attenuation function to suppress the raised peaks at the center of the shifted spectra

$$a_1(\mathbf{k}) = \begin{cases} 1 - A_{att} e^{-\frac{\mathbf{k}^2}{(0.5\bullet\sigma_{att})^2}}, m = \pm 1 \\ 1, m = 0 \end{cases} \tag{18}$$

where $A_{att}$ and $\sigma_{att}$ are respectively the attenuation strength and width. This attenuation function is similar to that of the conventional Wiener-SIM, except that the attenuation strength for the zero-order is set to zero, to avoid amplifying the residual out-of-focus background at the center of $\tilde{S}'_{directly-combined}(\mathbf{k})$. With the initial optimization, the abnormal features in $\tilde{S}'_{directly-combined}(\mathbf{k})$ can be well corrected, so the typical artifacts and residual background can be effectively eliminated.

Following the optimization, another deconvolution is employed to recover the high-frequency signals suppressed by the optimized OTF, which can be expressed as follows

$$\tilde{W}_2(\mathbf{k}) = \frac{\tilde{A}(\mathbf{k})}{\sum_m a_2(\mathbf{k}+m\mathbf{k}_d)\bullet\left|\tilde{H}(\mathbf{k}+m\mathbf{k}_d)\right|^2 + w_2^2} \tag{19}$$

where $w_2$ denotes another empirical parameter for the second Wiener deconvolution. Besides, the apodization function and the attenuation function were designed as

$$\tilde{A}(\mathbf{k}) = e^{-\frac{\mathbf{k}^2}{2(FWHM_{Apo}/\sqrt{2\ln 2})^2}} \tag{20}$$

$$a_2(\mathbf{k}) = \begin{cases} 1 - \frac{A_{att}}{1.15} e^{-\frac{\mathbf{k}^2}{(0.5\bullet\sigma_{att})^2}}, m = \pm 1 \\ 1 - \frac{A_{att}}{1.05} e^{-\frac{\mathbf{k}^2}{(0.5\bullet\sigma_{att})^2}}, m = 0 \end{cases} \tag{21}$$

in which $FWHM_{Apo}$ is the full width at half maximum (FWHM) of the apodization function $\tilde{A}(\mathbf{k})$, which was used to suppress artifacts caused by high-frequency noises. The attenuation strength in the second attenuation function is tuned slightly smaller to compensate for the over-attenuated signals in $\tilde{S}'_{directly-combined}(\mathbf{k})$, which not only improves the spatial resolution but also recovers the real sample signals lost during optimization. With the second deconvolution optimization, the reconstructed spectrum presents no significant abnormal features and the high-frequency signal is sufficiently enhanced, thereby being able to offer a high-fidelity SR-SIM image with minimal artifacts.

Finally, the high-fidelity super-resolution image can be obtained by transforming the optimized spectrum back into the spatial domain

$$I_{\text{HiFi-SIM}}(\mathbf{r}) = \mathcal{F}^{-1}[\tilde{S}'_{directly-conbined}(\mathbf{k}) * \tilde{W}_1(\mathbf{k}) * \tilde{W}_2(\mathbf{k})] \tag{22}$$

### 1.3 A brief introduction to JSFR-SIM

In our previous work[10], to improve the reconstruction speed of conventional Wiener-SIM, we have developed a rapid reconstruction algorithm termed Joint Spatial-Frequency Reconstruction (JSFR-SIM). This algorithm replaced most of the frequency calculations in Wiener-SIM with simple multiplication and summation calculations in real space, resulting in improved image reconstruction speed. As demonstrated by theoretical derivation, the results of JSFR-SIM are consistent with the conventional Wiener-SIM, which ensures that the speed increase of JSFR-SIM does not come at the expense of image quality or spatial resolution.

The workflow of JSFR-SIM can be summarized to be the following four procedures. As a preparation procedure, the coefficient functions $c_{d,i}(\mathbf{r})$ are calculated in advance with the parameters of the illumination field. Assuming the phase shifts are denoted as $k_0\delta_i \in \{0, \alpha, 2\alpha\}$, a general form of $c_{d,i}(\mathbf{r})$ could be derived to be the following equations

$$\begin{aligned}
c_{d,1}(\mathbf{r}) &= \frac{1}{2(1-\cos\alpha)} + \frac{1-2\cos\alpha}{2(1-\cos\alpha)} m_d \cos(\mathbf{k}_d \bullet \mathbf{r} + \varphi_{d,0}) - \frac{2\cos\alpha + 1}{2\sin\alpha} m_d \sin(\mathbf{k}_d \bullet \mathbf{r} + \varphi_{d,0}) \\
c_{d,2}(\mathbf{r}) &= -\frac{\cos\alpha}{1-\cos\alpha} + \frac{\cos\alpha}{1-\cos\alpha} m_d \cos(\mathbf{k}_d \bullet \mathbf{r} + \varphi_{d,0}) + \frac{1+\cos\alpha}{\sin\alpha} m_d \sin(\mathbf{k}_d \bullet \mathbf{r} + \varphi_{d,0}) \\
c_{d,3}(\mathbf{r}) &= \frac{1}{2(1-\cos\alpha)} - \frac{1}{2(1-\cos\alpha)} m_d \cos(\mathbf{k}_d \bullet \mathbf{r} + \varphi_{d,0}) - \frac{1}{2\sin\alpha} m_d \sin(\mathbf{k}_d \bullet \mathbf{r} + \varphi_{d,0})
\end{aligned} \tag{23}$$

where $\varphi_{d,0}$ is the initial phase of the pattern in the $d$th ($d$ = 1,2,3) orientation.

Firstly, the raw images $D_{d,i}(\mathbf{r})$ are filtered with the attenuated OTF $a(\mathbf{k})\tilde{H}^*(\mathbf{k})$

$$D^f_{d,i}(\mathbf{r}) = \mathcal{F}^{-1}\left\{\tilde{D}_{d,i}(\mathbf{k}) \bullet [a(\mathbf{k})\tilde{H}^*(\mathbf{k})]\right\} \tag{24}$$

Next, an intermediate image is obtained by multiplying the pre-calculated coefficient functions with the corresponding filtered raw images and summing the results up

$$I^{intermediate}_{d,i}(\mathbf{r}) = \sum_{d=1}^{3}\sum_{i=1}^{3} c_{d,i}(\mathbf{r}) D^f_{d,i}(\mathbf{r}) \tag{25}$$

In the end, the final super-resolution image can be directly recovered by completing the Wiener deconvolution

$$I_{\text{JSFR-SIM}}(\mathbf{r}) = \mathcal{F}^{-1}\left\{\mathcal{F}\left[I_{d,i}^{intermediate}(\mathbf{r})\right] * \tilde{W}_0(\mathbf{k})\right\} \tag{26}$$

where $\tilde{W}_0(\mathbf{k})$ is the deconvolution factor the same as that of Wiener-SIM (see Eq. (14))

**1.4 Principle of JSFR-AR-SIM**

In this paper, to accelerate the reconstruction of HiFi-SIM, we first replace the iterative Richardson-Lucy (RL) deconvolution with a Wiener-type filter, for it would be too time-consuming to implement the RL deconvolution for each raw image. Secondly, we extend the concept of joint spatial-frequency domain reconstruction to the HiFi-SIM workflow, with which most spectral operations would be converted to lightweight point multiplication and summation in real space. More importantly, by combining the above Wiener-type filter with the first step of JSFR-SIM (see Eq. (24)), the computation power required by RL deconvolution is eliminated. Besides, we move all calculations irrelevant to specimen distribution to the preparation procedure, which greatly reduces redundancy calculations for consecutive reconstructions, as we did in JSFR-SIM.

a) Replacement of the time-consuming RL deconvolution

Considering the image forward model of SR-SIM in Eq. (1), the results of RL deconvolution in the preprocessing procedure of HiFi-SIM are a maximum likelihood estimation of the pattern-illuminated object $O(\mathbf{r})\bullet I_{d,i}(\mathbf{r})$ under non-negative prior[11-13]. With limited iterations (typically 5 iterations in HiFi-SIM), such estimation that stopped far before convergence is more like an enhancement of high-frequency information, which can also be achieved by the non-iterative Wiener deconvolution method constructed with least square estimation[11]. As a likelihood estimation of the sample, the RL deconvolution generally reveals a larger expansion in the recovered spectrum than the conventional Wiener deconvolution, as shown in Fig. S2.

However, all the preprocessed raw images will subsequently be processed with a bandpass filter $a(\mathbf{k})\tilde{H}^*(\mathbf{k})$ to implement the OTF compensation and OTF attenuation in the main reconstruction procedures, with which the extra spectrum information gained by RL deconvolution will be suppressed by the bandpass filter. As such, the RL deconvolution does not provide any extra spectrum information of the sample than a Wiener-type filter, as illustrated by Fig. S2. Therefore, it makes sense for us to replace the RL deconvolution in the preprocessing procedure[11,14] with a Wiener-type filter to accelerate the reconstruction.

As such, the preprocessed raw images $D'_{d,i}(\mathbf{r})$ in HiFi-SIM (see Eq. (15)) could be replaced by

$$D'_{d,i}(\mathbf{r}) = \mathcal{F}^{-1}\left[\tilde{D}_{d,j}(\mathbf{k})\bullet\tilde{W}_{\mathrm{p}}(\mathbf{k})\right] \tag{27}$$

where $W_{\mathrm{p}}(\mathbf{k})$ is a Wiener-type filter for the preprocessing procedure, which can be expressed by

$$\tilde{W}_{\mathrm{p}}(\mathbf{k}) = \frac{\tilde{H}^*(\mathbf{k})}{\left|\tilde{H}(\mathbf{k})\right|^2 + w_{\mathrm{p}}^{\,2}} \tag{28}$$

in which $w_{\mathrm{p}}$ is the Wiener parameter in the preprocessing procedure, which can be set as 0.1 by default. As expected, we found no significant change in image quality after replacing the RL deconvolution in HiFi-SIM with a Wiener-type filter (see Fig. S3).

b) Fusion with the rapid JSFR-SIM method

Except for the initial RL deconvolution and the final two-step optimization, the main procedures of HiFi-SIM are the same as that of conventional Wiener-SIM including the band separation, band shifting, band superposition, OTF compensation, and OTF attenuation. Therefore, the reconstruction strategies in JSFR-SIM can be directly extended to the HiFi-SIM workflow. Thereinto, as demonstrated in JSFR-SIM, the OTF compensation procedure and the OTF attenuation procedure in Wiener-SIM are equivalent to a preset band-pass filter to the raw images, as shown in Eq. (24).

In our JSFR-AR-SIM workflow, the raw images will first be filtered by the Wiener-type filter as Eq. (27) for preprocessing and then filtered by the band-pass filter in Eq. (24) to realize OTF compensation and OTF attenuation, that is,

$$D'_{d,i}(\mathbf{r}) = \mathcal{F}^{-1}\left( \mathcal{F}[D_{d,i}(\mathbf{r})] \bullet \frac{\tilde{H}^*(\mathbf{k})}{\left|\tilde{H}(\mathbf{k})\right|^2 + w_{\mathrm{p}}{}^2} \right) \tag{29}$$

$$D'^{f}_{d,i}(\mathbf{r}) = \mathcal{F}^{-1}\left\{ \mathcal{F}[D'_{d,i}(\mathbf{r})] \bullet [a(\mathbf{k})\tilde{H}^*(\mathbf{k})] \right\} \tag{30}$$

By substituting Eq. (29) into Eq. (30), these two filters can easily be combined to be a composite filter

$$\tilde{G}(\mathbf{k}) = \frac{\tilde{H}^*(\mathbf{k})}{\left|\tilde{H}(\mathbf{k})\right|^2 + w_{\mathrm{p}}{}^2} \bullet a(\mathbf{k})\tilde{H}^*(\mathbf{k}) \tag{31}$$

As such, the raw images after preprocessing, OTF compensation, and OTF attenuation becomes

$$D'^{f}_{d,i}(\mathbf{r}) = \mathcal{F}^{-1}\left\{ \mathcal{F}[D_{d,i}(\mathbf{r})] \bullet \tilde{G}(\mathbf{k}) \right\} \tag{32}$$

Subsequently, as in JSFR-SIM, a new intermediate SR image can be obtained by multiplying the pre-calculated coefficient functions (Eq. (23)) with the filtered raw images and summing the results up

$$I'^{intermediate}_{d,i}(\mathbf{r}) = c_{d,i}(\mathbf{r}) D'^{f}_{d,i}(\mathbf{r}) \tag{33}$$

c) Exclusion of the redundancy computing for consecutive reconstructions

After the above modifications, the final two-step optimization remains to be the most computationally expensive procedure in the HiFi-SIM workflow. Fortunately, these two optimization functions can be calculated in advance by only using the estimated illumination parameters. Also, they can be reused for consecutive reconstructions. Therefore, the computation of the optimization functions $\tilde{W}_1(\mathbf{k})$ and $\tilde{W}_2(\mathbf{k})$ can be moved to preprocessing procedures, with which their execution time could be excluded in consecutive reconstructions. Considering the two optimization functions are successively multiplied with the directly combined spectrum, they can be combined into a single function for sake of convenience

$$\tilde{W}(\mathbf{k}) = \tilde{W}_1(\mathbf{k}) \bullet \tilde{W}_2(\mathbf{k}) \quad (34)$$

where $\tilde{W}_1(\mathbf{k})$ and $\tilde{W}_2(\mathbf{k})$ can be respectively obtained by Eq. (17) and Eq. (19).

The final super-resolution image is recovered by completing the spectrum optimization

$$I_{\text{JSFR-AR-SIM}}(\mathbf{r}) = \mathcal{F}^{-1}\left\{\mathcal{F}\left[\sum_{d=1}^{3}\sum_{i=1}^{3} I_{d,i}^{\prime intermediate}(\mathbf{r})\right] * \tilde{W}(\mathbf{k})\right\} \quad (35)$$

### 1.5 Workflow of JSFR-AR-SIM

After the above modifications, the implementation of JSFR-AR-SIM can easily be summarized as follow:

| **Algorithm: JSFR-AR-SIM** |
|---|
| **Initialization and Preparation:** |
| Estimate the illumination parameters $\mathbf{k}_d$, $\varphi_d$, $m_d$; |
| Calculate the coefficient functions $c_{d,i}(\mathbf{r})$ with Eq. (23); |
| Obtain the optimization function $W(\mathbf{k})$ with Eq. (34) |
| **Main Reconstruction:** |
| **Step 1:** Calculate the filtered raw images with Eq. (32). |
| **Step 2:** Compute the intermediate SR image by Eq. (33). |
| **Step 3:** Obtain the final artifact-reduced SR image with Eq. (35). |

In other words, the revised workflow only contains three main procedures: Firstly, all the raw images are filtered by using the composite filter. Secondly, an intermediate SR image is obtained by superimposing the dot products of the filtered raw images and the pre-calculated coefficient functions. Finally, the artifact-reduced SR image is recovered by multiplying the frequency spectrum of the intermediate SR image with the combined optimization function $\tilde{W}(\mathbf{k})$ and transferring the optimized spectrum back to real space. The computation involved in this method is significantly less than HiFi-SIM, nearly the same to be previous JSFR-SIM. A more detailed illustration of the algorithm can be found in Fig. 1 of the main manuscript.

## Supplementary Note 2. Single-layer 3D-SIM reconstruction in real space

The JSFR-AR-SIM method is also compatible with single-layer 3D-SIM data. The main difference is the number of the raw images and phase shifts in each orientation, which were generally set as 5 for 3D-SIM (3 for 2D-SIM). As such, to extend this method for the reconstruction of single-layer 3D-SIM datasets, we have to change the range of the phase index $i$ ($i$ = 1,2,3) to $i$ ($i$ = 1,2,3,4,5) in the above equations (including Eqs. (32), (33), and (35)).

Besides, the coefficient functions in Eq. (23) should be revised to

$$\begin{pmatrix} c_{d,1}(\mathbf{r}) \\ c_{d,2}(\mathbf{r}) \\ c_{d,3}(\mathbf{r}) \\ c_{d,4}(\mathbf{r}) \\ c_{d,5}(\mathbf{r}) \end{pmatrix} = \begin{pmatrix} 1 & 1 & 1 & 1 & 1 \\ 1 & \cos\Delta\varphi_{d,1} & \cos\Delta\varphi_{d,2} & \cos\Delta\varphi_{d,3} & \cos\Delta\varphi_{d,4} \\ 0 & \sin\Delta\varphi_{d,1} & \sin\Delta\varphi_{d,2} & \sin\Delta\varphi_{d,3} & \sin\Delta\varphi_{d,4} \\ 1 & \cos2\Delta\varphi_{d,1} & \cos2\Delta\varphi_{d,2} & \cos2\Delta\varphi_{d,3} & \cos2\Delta\varphi_{d,4} \\ 0 & \sin2\Delta\varphi_{d,1} & \sin2\Delta\varphi_{d,2} & \sin2\Delta\varphi_{d,3} & \sin2\Delta\varphi_{d,4} \end{pmatrix}^{-1} \begin{pmatrix} \frac{1}{I_0} \\ \frac{1}{m_1 I_0}\cos(\mathbf{k}_d \bullet \mathbf{r} + \varphi_{d,0}) \\ \frac{1}{m_1 I_0}\sin(\mathbf{k}_d \bullet \mathbf{r} + \varphi_{d,0}) \\ \frac{1}{m_2 I_0}\cos(2\mathbf{k}_d \bullet \mathbf{r} + 2\varphi_{d,0}) \\ \frac{1}{m_2 I_0}\sin(2\mathbf{k}_d \bullet \mathbf{r} + 2\varphi_{d,0}) \end{pmatrix} \tag{36}$$

where $\varphi_{d,0}$ is the initial phase of the pattern in the $d$th ($d$ = 1,2,3) orientation, and the phase shifts in each orientation are denoted as $k_0\delta_i \in \{0, \Delta\varphi_{d,1}, \Delta\varphi_{d,2}, \Delta\varphi_{d,3}, \Delta\varphi_{d,4}\}$.

As to the optimization functions, the range of the component index $m$ ($m$ = 0, ±1) in Eqs. (17) and (19) should be changed to $m$ ($m$ = 0, ±1, ±2). Similar to the HiFi-SIM method, the attenuation function in the second optimization is also modified as

$$a_2(\mathbf{k}) = \begin{cases} \frac{1}{1.2}\left(1 - A_{att} e^{-\frac{\mathbf{k}^2}{(0.5\bullet\sigma_{att})}}\right), m = \pm1, \pm2 \\ 1 - \frac{A_{att}}{1.05} e^{-\frac{\mathbf{k}^2}{(0.5\bullet\sigma_{att})}}, m = 0 \end{cases} \tag{37}$$

After these modifications, we can directly use the workflow in Supplementary Note 1 to reconstruct single-layer 3D-SIM data, as demonstrated by Figs. S8-S9.

## References


1. O'Holleran K, Shaw M. Optimized approaches for optical sectioning and resolution enhancement in 2D structured illumination microscopy. *Biomed Opt Express* **5**, 2580-2590 (2014).
2. Demmerle J*, et al.* Strategic and practical guidelines for successful structured illumination microscopy. *Nat Protoc* **12**, 988-1010 (2017).
3. Fan J, Huang X, Li L, Tan S, Chen L. A protocol for structured illumination microscopy with minimal reconstruction artifacts. *Biophys Rep* **5**, 80-90 (2019).
4. Wen G*, et al.* High-fidelity structured illumination microscopy by point-spread-function engineering. *Light Sci Appl* **10**, 1-12 (2021).
5. Gustafsson MG*, et al.* Three-dimensional resolution doubling in wide-field fluorescence microscopy by structured illumination. *Biophys J* **94**, 4957-4970 (2008).
6. Wicker K. Non-iterative determination of pattern phase in structured illumination microscopy using auto-correlations in Fourier space. *Opt Express* **21**, 24692-24701 (2013).
7. Zhou X*, et al.* Image recombination transform algorithm for superresolution structured illumination microscopy. *J Biomed Opt* **21**, 096009 (2016).
8. Cao R*, et al.* Inverse matrix based phase estimation algorithm for structured illumination microscopy. *Biomed Opt Express* **9**, 5037-5051 (2018).
9. Zhao T*, et al.* Multi-color structured illumination microscopy for live cell imaging based on the enhanced image recombination transform algorithm. *Biomed Opt Express* **12**, 3474-3484 (2021).
10. Wang Z*, et al.* High-speed image reconstruction for optically sectioned, super-resolution structured illumination microscopy. *Adv Photon* **4**, 026003 (2022).
11. Sibarita J-B. Deconvolution microscopy. In: *Microscopy Techniques* (ed Rietdorf J). Springer Berlin Heidelberg (2005).
12. Richardson WH. Bayesian-based iterative method of image restoration. *J Opt Soc Am* **62**, 55-59 (1972).
13. Lucy LB. An iterative technique for the rectification of observed distributions. *Astron J* **79**, 745 (1974).
14. Zhao W*, et al.* Sparse deconvolution improves the resolution of live-cell super-resolution fluorescence microscopy. *Nat Biotechnol* **40**, 606-617 (2022).

# Supplementary Figures

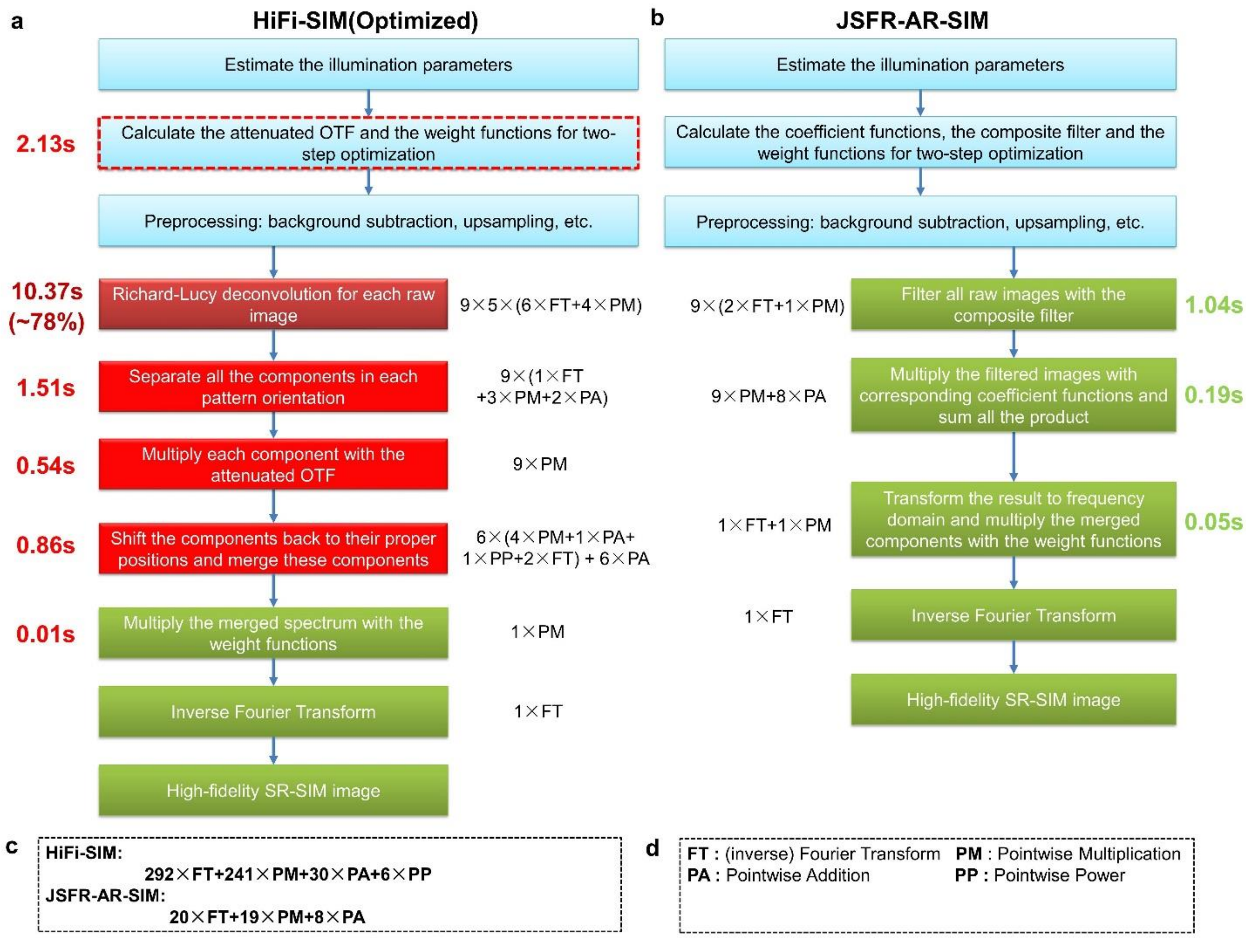


**Supplementary Figure 1. Comparison of the workflow of HiFi-SIM and JSFR-AR-SIM.** (a) The workflow of the rearranged HiFi-SIM. As the original HiFi-SIM workflow was not specially designed for fast reconstruction, we rearranged its reconstruction procedures to provide a fair comparison with the JSFR-AR-SIM. (b) The workflow of the JSFR-AR-SIM. To provide an intuitionistic impression of the source of computing burden, the image calculations and the execution time of each main procedure in the two algorithms is listed beside the diagrams. The latter was tested in CPU (Intel Core i7-9700K) with a raw image size of 1024×1024. (c) Comparison of the computing burden of HiFi-SIM and JSFR-AR-SIM. (d) Definition of the symbols in panels a-c.

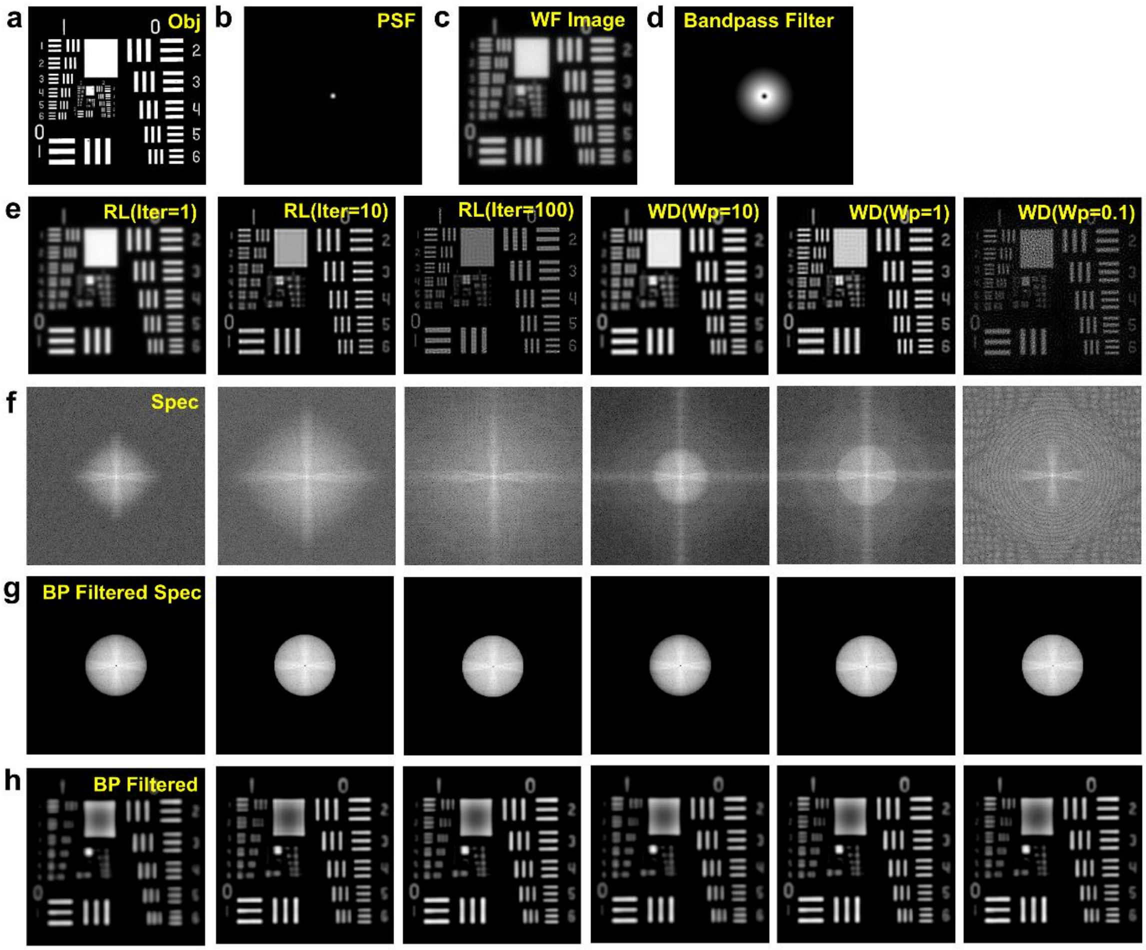


**Supplementary Figure 2. The bandpass filtering weakens the influence of deconvolution methods and deconvolution parameters in the preprocessing procedure.** As the preprocessing procedure and the subsequent bandpass filtering are identical to all raw images, without loss of generality, we directly use a widefield image to present the influence of deconvolution methods and deconvolution parameters. Firstly, a synthetic widefield image (c) is generated by convoluting the simulative object (a) with the PSF of the microscope (b). Then, it is respectively deconvoluted with Richardson-Lucy algorithm (RL) and Wiener deconvolution (WN) with varying parameters, as shown in (e). The insets in (e) respectively denote the RL results with 1, 10, and 100 iterations and the WD results with the deconvolution parameter of 10, 1, and 0.1 from left to right. Panels (f), (g), and (h) respectively present the spectrums, the bandpass filtered spectrums, and the bandpass filtered images of the deconvoluted images in (e). As expected, with sufficient iterations, the RL method can recover more spectrum information than the Wiener deconvolution. However, after the bandpass filtering, the advantage of RL is tremendously weakened, as demonstrated by both the spectrums and images in (g) and (h). Moreover, the influence of the deconvolution parameters (including the iteration numbers in the RL algorithm and the Wiener parameter in Wiener deconvolution) in the final image is also greatly suppressed, which explains why HiFi-SIM can use a small iteration number (typically 5) in the preprocessing.

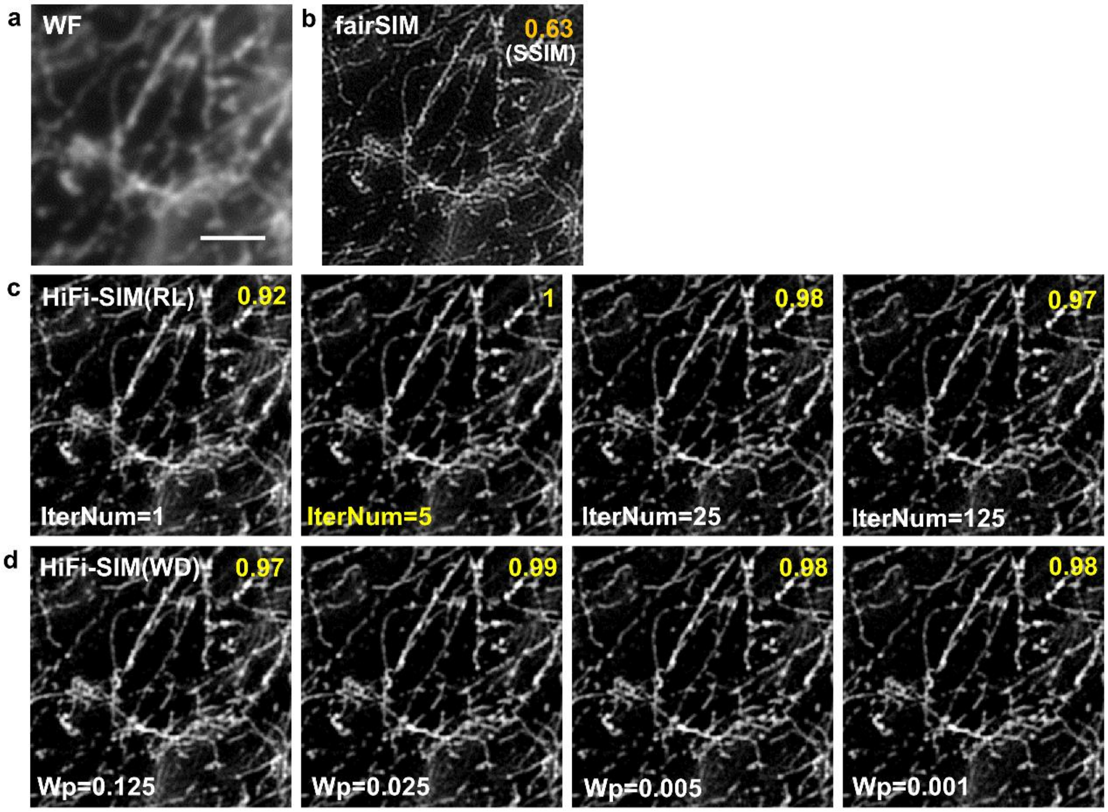


**Supplementary Figure 3. Replacing the Richardson-Lucy algorithm with the Wiener deconvolution in the preprocessing step of HiFi-SIM does not significantly affect the image quality of the final image.** (a) and (b) are respectively the pseudo-widefield image and the SR image recovered by fairSIM of microtubules in fixed COS-7 cells. (c) and (d) are the SR images reconstructed by HiFi-SIM with the RL algorithm and the Wiener deconvolution in the preprocessing procedure, with varying deconvolution parameters. The numbers at the upper-right corner in the insets of (b)-(d) indicate the structural similarity of the current image, comparing with the original HiFi-SIM image. Scale bar: 2 μm.

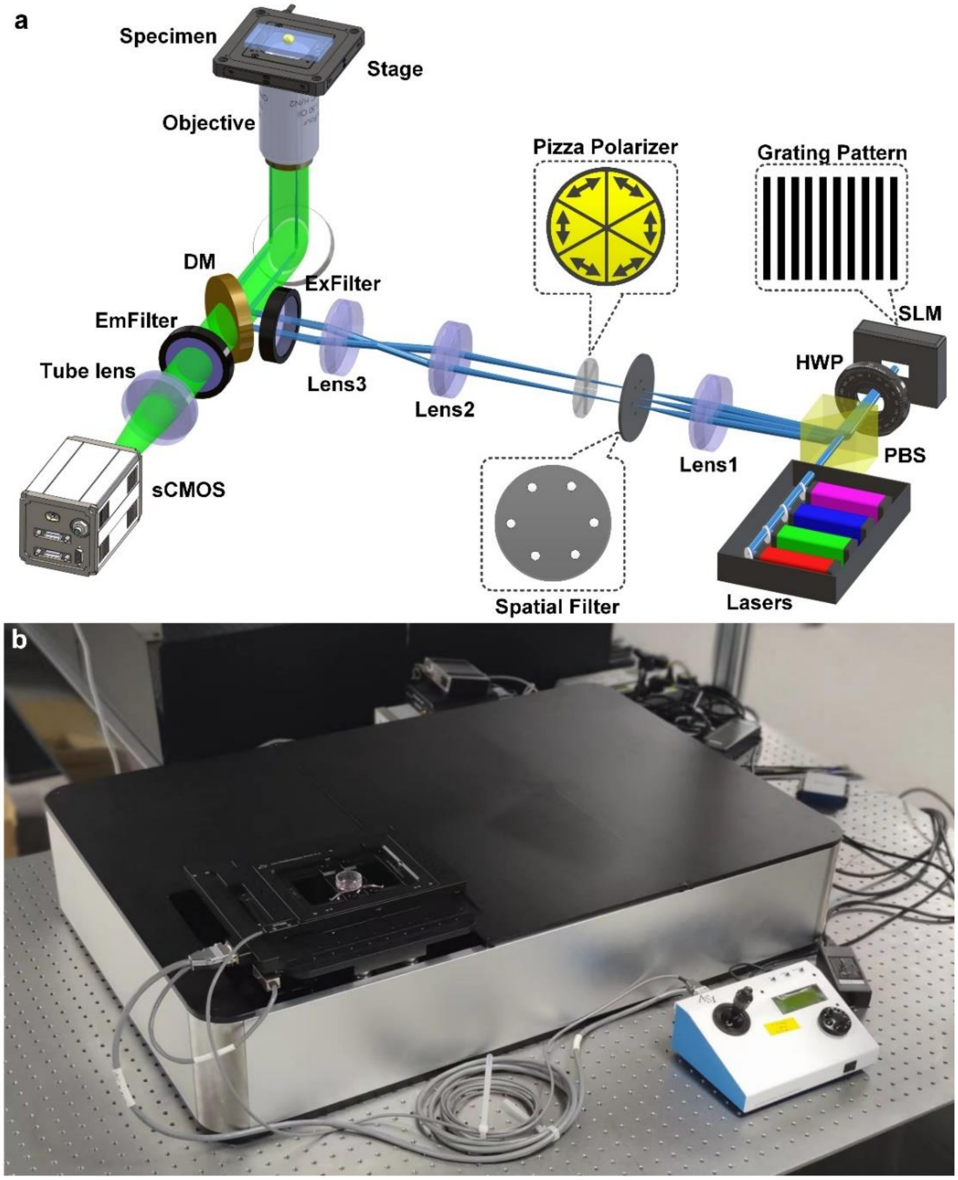


**Supplementary Figure 4. Layout of the custom-built SR-SIM setup.** (a) Light path of the 2D-SIM system. The expanded and collimated light from a multiwavelength laser (405nm, 488nm, 561nm, and 638nm) was first diffracted into various orders after being modulated by the SLM. Afterward, the ±1-orders diffraction orders are selected with a spatial filter. To maximize the modulation depth of the illumination pattern, we designed a pizza-shape linear polarizer and placed it after the stop mask, eliminating the switching time between different pattern orientations. These two coherent beams are then relayed onto the back focal plane of the microscope objective, producing sinusoidal patterns on the specimen. PBS: polarized beam splitter; SLM: spatial light modulator; HWP: half-wave plate; ExFilter: excitation filter; EmFilter: emission filter; DM: dichroic mirror. (b) A photograph of the custom-built SR-SIM setup.

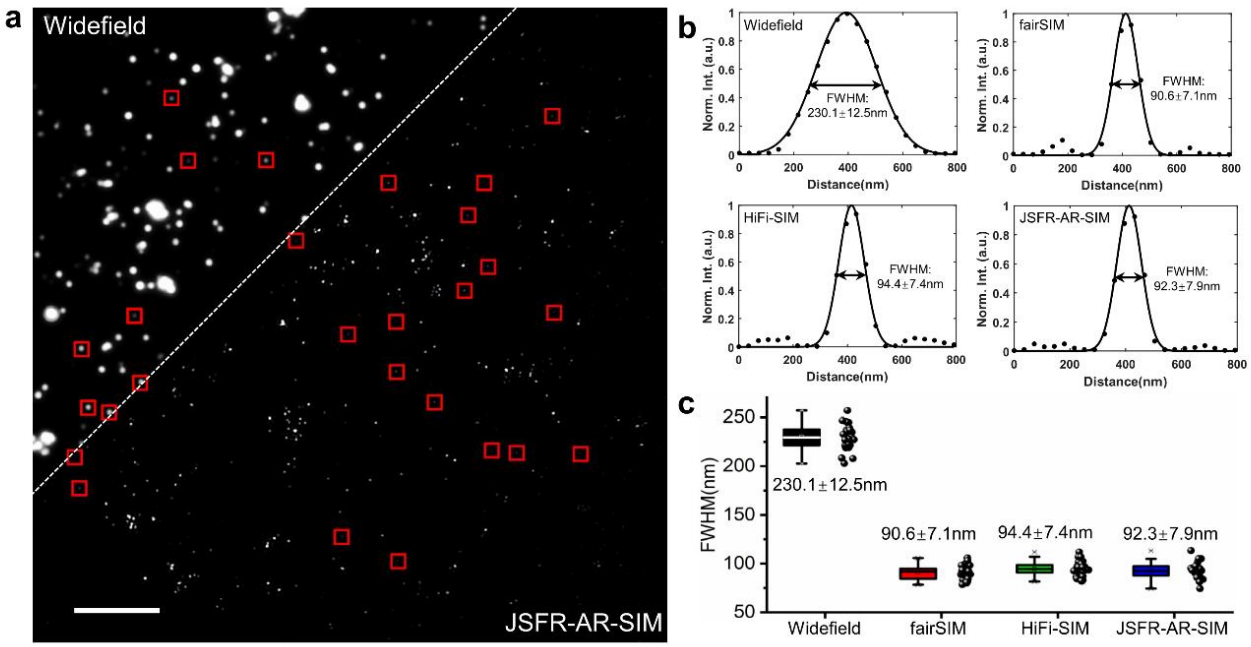


**Supplementary Figure 5. The resolution performance of JSFR-AR-SIM is validated by isolated fluorescent nanobeads.** (a) Widefield image (right-top corner) and SR image recovered with JSFR-AR-SIM of the 40 nm diameter fluorescent beads in Fig. 2. To calibrate the spatial resolution, thirty isolated nanobeads were manually selected, whose intensity profiles were subsequently extracted and fit to Gaussian functions. (b) The intensity data and the fitted Gaussian curves of a representative fluorescent nanobead respectively recovered with pseudo-widefield, JSFR-SIM, HiFi-SIM, and JSFR-AR-SIM along the x-axes. (c) is the statistical result of the FWHM of the fluorescent beads. Note that the resolution of the JSFR-AR-SIM method is comparable to that of JSFR-SIM. Scale bars: (a) 5 μm.

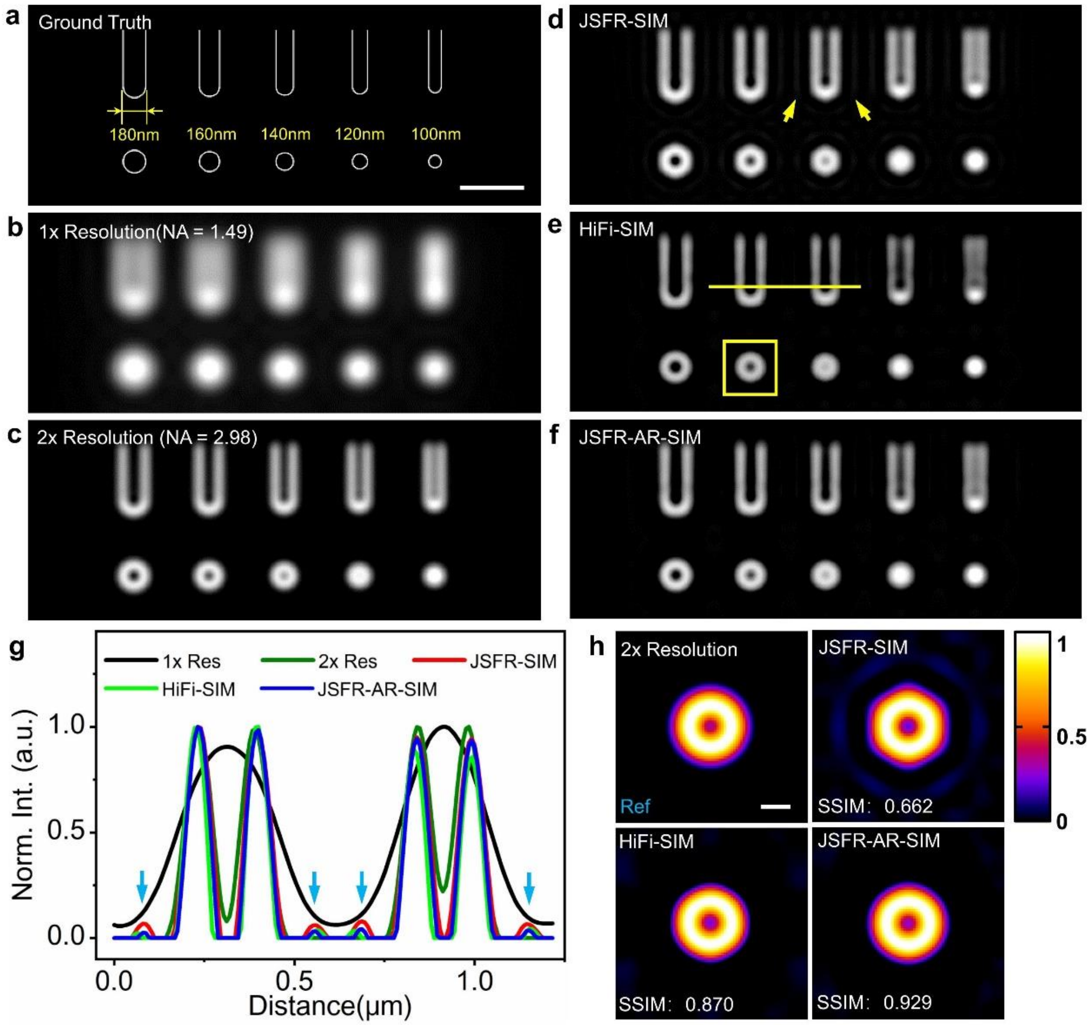


**Supplementary Figure 6. Simulative results of rings and line pairs.** (a) Synthetic rings (bottom, line width: 4 nm) and line pairs (top, line width: 4 nm) with a diameter of 180 nm, 160 nm, 140 nm, 120 nm, and 100 nm are generated as ground-truth. (b) and (c) are respectively the synthetic widefield image and ideal super-resolution image generated by convoluting the ground truth image with diffraction-limited PSF (NA=1.49) and super-resolution PSF (NA=2.98). The original pixel sizes of the ground truth image and the PSFs were set to be 1 nm, which was subsequently subsampled to obtain a pitch size of 16 nm in the final images. At the same time, nine synthetic raw SIM images were obtained by multiplying the ground truth image with nine fringe patterns (period: 1.2×FWHM, 3 orientations, 3 phases) and then convoluting with the diffraction-limited PSF. (d)-(f) are SR images recovered with JSFR-SIM, HiFi-SIM, and the developed JSFR-AR-SIM. (g) The intensity profiles of the widefield image and SR images recovered with JSFR-SIM, HiFi-SIM, and JSFR-AR-SIM along the yellow solid lines in (e). The JSFR-SIM image presents sidelobes with nearly 9% brightness, which became less than 2% in HiFi-SIM and JSFR-AR-SIM, as indicated by the blue arrows. (h) The magnified views of ring-shaped structure at the yellow-boxed region of (e). Treating the ideal SR image as the reference, the SSIM value of JSFR-SIM, HiFi-SIM, and JSFR-AR-SIM was measured to be 0.662, 0.870, 0.929. Noted that the ring structure recovered by JSFR-SIM presents slight anisotropy, while the HiFi-SIM and JSFR-AR-SIM results show better symmetry. (a)-(f) 500 nm; (h) 100 nm.

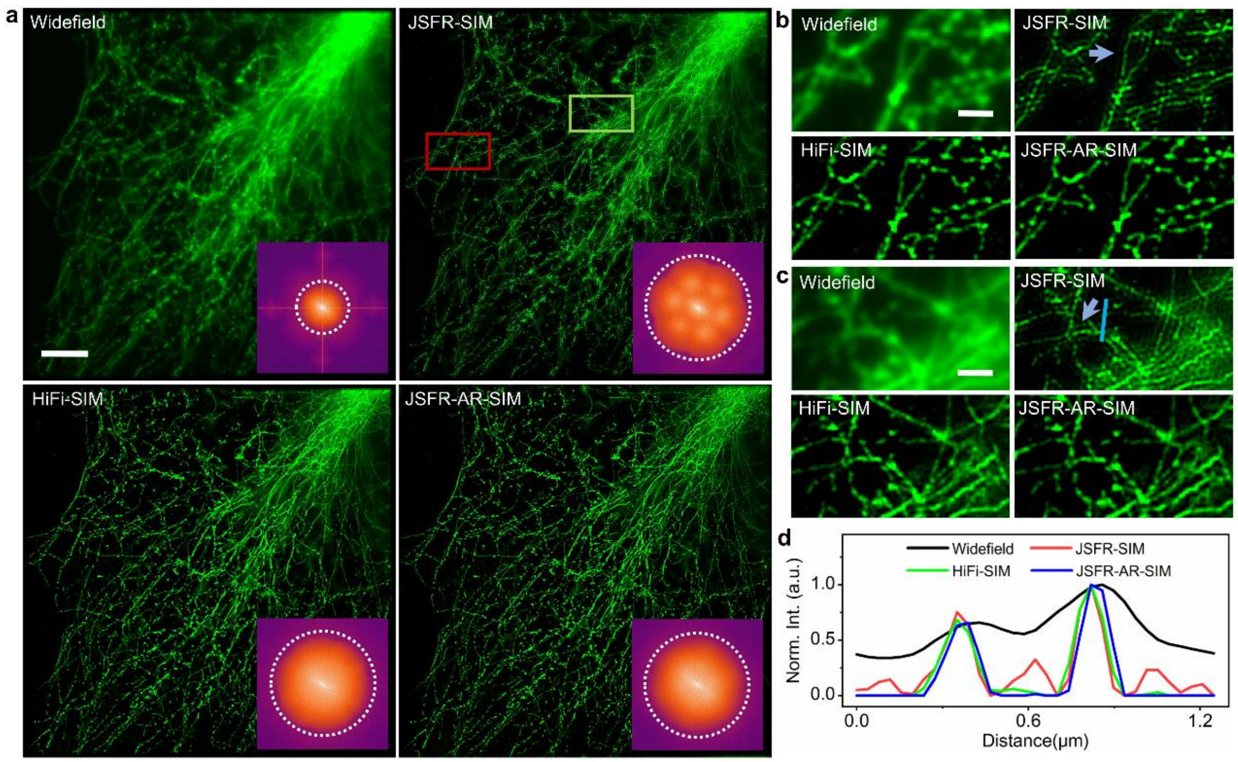


**Supplementary Figure 7. The performance of JSFR-AR-SIM is identical to HiFi-SIM in suppressing sidelobe artifacts.** (a) Pseudo-widefield image and SR images of microtubules in fixed COS-7 cells. The SR images are respectively reconstructed by JSFR-SIM, HiFi-SIM, and JSFR-AR-SIM. (b) and (c) are the magnified views of the pseudo-widefield image and SR images of the lines in the red- and green-boxed region of (a). The abnormal artifacts induced by JSFR-SIM is effectively suppressed by the developed JSFR-AR-SIM and the previous HiFi-SIM, resulting in significantly improved image quality. (d) The intensity profiles of the images along the blue solid lines in (c). Scale bars: (a) 5 μm; (b)-(c) 1 μm.

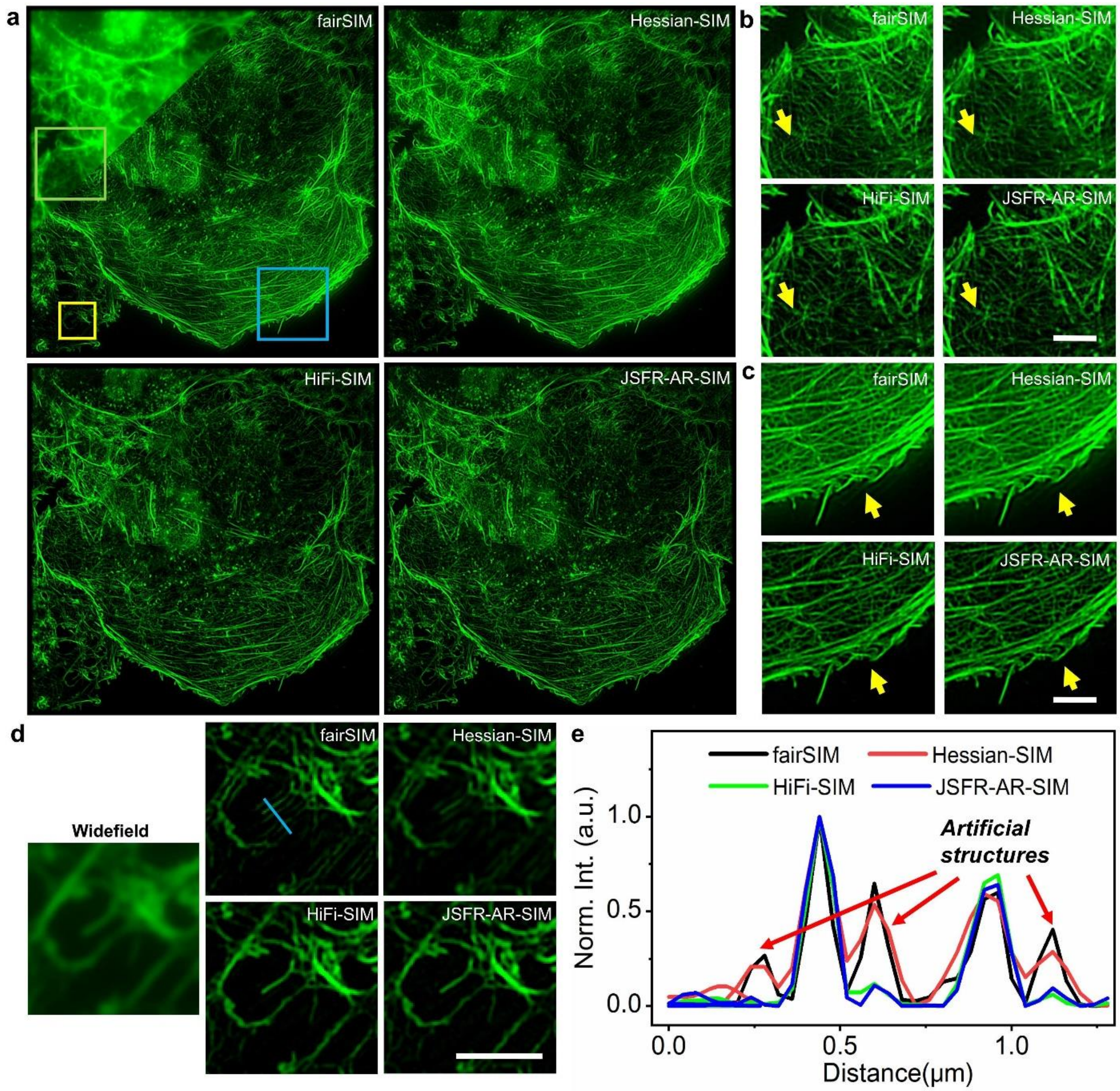


**Supplementary Figure 8. JSFR-AR-SIM enables artifact-reduced reconstruction on single slice 3D-SIM raw data.** The raw 3D-SIM data (the fifth slice of OMX_LSEC_Actin_525nm.tif) is downloaded from the fairSIM website, which imaged actin filaments in the liver sinusoidal endothelial cells (LSECs). (a) SR images reconstructed by fairSIM (strength 0.99, FWHM 1.2 cycles/micron, Wiener parameter 0.1), Hessian-SIM, HiFi-SIM and JSFR-AR-SIM. The Hessian-SIM result is reprocessed from the fairSIM result, using the Hessian-denoising code provided by Huang et. al. (b)-(d) are respectively the magnified views of these SR images at the green-, blue- and yellow-boxed region in (a). The obvious sidelobe artifacts induced by fairSIM are difficult to be eliminated by the Hessian-SIM method, which, however, is effectively suppressed by the developed JSFR-AR-SIM and the previous HiFi-SIM, resulting in significantly improved fidelity. The maximal intensities of the magnified views are simultaneously adjusted to present the details. (e) The intensity profiles of the filaments along the blue line in (e) for different reconstruction algorithms. Scale bars: (a) 5 μm; (b)-(d) 2 μm.

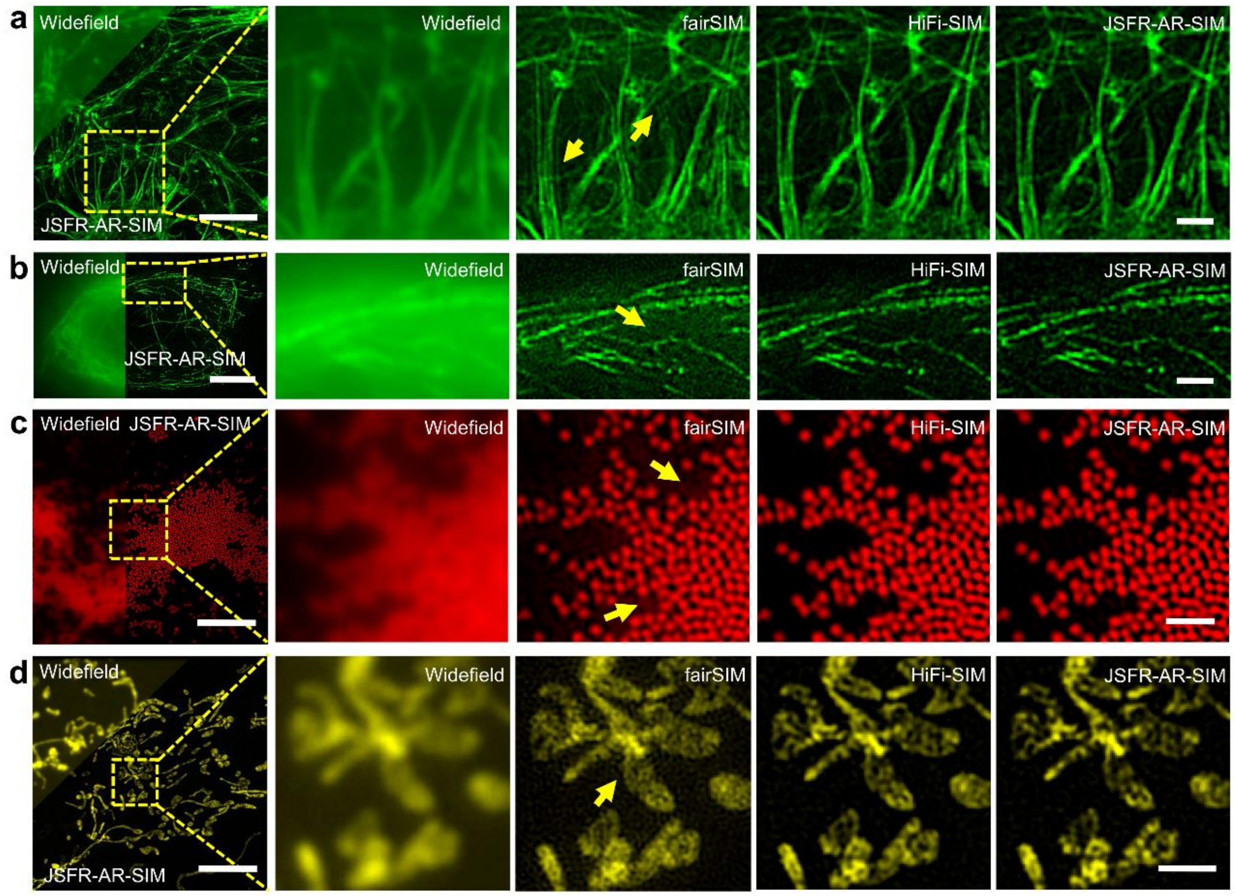


**Supplementary Figure 9. Performance tests of JSFR-AR-SIM on reconstructing open-source datasets downloaded from the fairSIM website.** For all datasets, the left column displays the pseudo-widefield image and the SR image reconstructed by JSFR-AR-SIM, while the right four columns respectively present the magnified view of the pseudo-widefield image and SR images reconstructed by fairSIM, HiFi-SIM, and JSFR-AR-SIM in the yellow-boxed region of the left column. (a) SR images of actin filaments in liver sinusoidal endothelial cells (OMX_LSEC_Actin_525nm.tif). The obvious sidelobe artifacts produced by JSFR-SIM are effectively suppressed, resulting in significantly improved fidelity. (b)-(c) SR images of microtubule in U2OS cells (OMX_U2OS_Tubulin_525nm.tif) and 200nm-diameter microspheres of (SLM-SIM_Tetraspeck200_680nm.tif) demonstrate the superior performance of JSFR-AR-SIM and HiFi-SIM in suppressing the residual background and the grainy artifacts caused by the strong background fluorescence. (d) SR images of mitochondria in U2OS cells (Zeiss_Mito_600nm_large.tif). Note that JSFR-AR-SIM and HiFi-SIM generate "cleaner" SR images with individual mitochondrial features much easier to be identified. All these raw datasets as well as the detailed imaging parameters can be found and freely downloaded on the fairSIM website. Scale bar: Left column in (a)-(d), 5 μm; Right four columns in (a)-(d), 1 μm.